Supplementary modeling (SM)

Supplementary modeling (SM) movie legends

Supporting movie SM1
Interactions between amylin (magenta) and the ECD of CTR in complex with RAMP1, during a SuMD simulation (SuMD simulation time 0-16 ns ca.) and the following unsupervised MD (16 ns ca. - end of the simulation). Right hand panel interactively shows the computed interaction energy during the simulation. The receptor is shown as ribbon, with key residues in stick and color-coded according to the number of contacts computed on overall 10 SuMD replicas: in blue are depicted residues never engaged by the peptide, while in red are highlighted residues frequently engaged (the color scale is normalized on the residue mostly engaged).

Supporting movie SM2
Interactions between amylin (magenta) and the ECD of CTR, during one SuMD simulation (SuMD simulation time 0-15 ns ca.) and the following unsupervised MD (15 ns - end of the simulation). Right hand panel interactively shows the computed interaction energy during the simulation. The receptors is shown as ribbon, with key residues in stick and color-coded according to the number of contacts computed on overall 12 SuMD replicas: in blue are depicted residues never engaged by the peptide, while in red are highlighted residues frequently engaged (the color scale is normalized on the residue mostly engaged).

Supporting movie SM3
Interactions between AMY_1 (left hand panel) or CTR (right hand panel) with amylin (magenta), during a 250 ns long MD replica. Receptors are shown as ribbon, with key residues in stick and color-coded according to the number of contacts computed on overall 750 ns of simulations (3 MD replicas): in blue are depicted residues never engaged by the peptide, while in red are highlighted residues frequently engaged (the color scale is normalized on the residue mostly engaged).

Supporting movie SM4
Interactions between AMY_1 (left hand panel) or CTR (right hand panel) with the N terminus portion of amylin (magenta), during a 250 ns long MD replica. Receptors are shown as ribbon, with key residues in stick and color-coded according to the number of contacts computed on overall 750 ns of simulations (3 MD replicas): in blue are depicted residues never engaged by the peptide, while in red are highlighted residues frequently engaged (the color scale is normalized on the residue mostly engaged).

Supporting movie SM5
Amylin (magenta) partial unbinding from AMY_1 (left hand panel) or CTR (right hand panel) under the input of energy. Receptors are shown as ribbon, with key residues in stick and color-coded according to the number of contacts computed on overall 3 metadynamics replicas: in blue are depicted residues never engaged by the peptide, while in red are highlighted residues frequently engaged (the color scale is normalized on the residue mostly engaged).

Supporting movie SM6
Interactions between amylin Q10A mutant (magenta) and AMY_1, during a 100 ns long MD replica. The receptor is shown as blue ribbon, with key residues in stick.

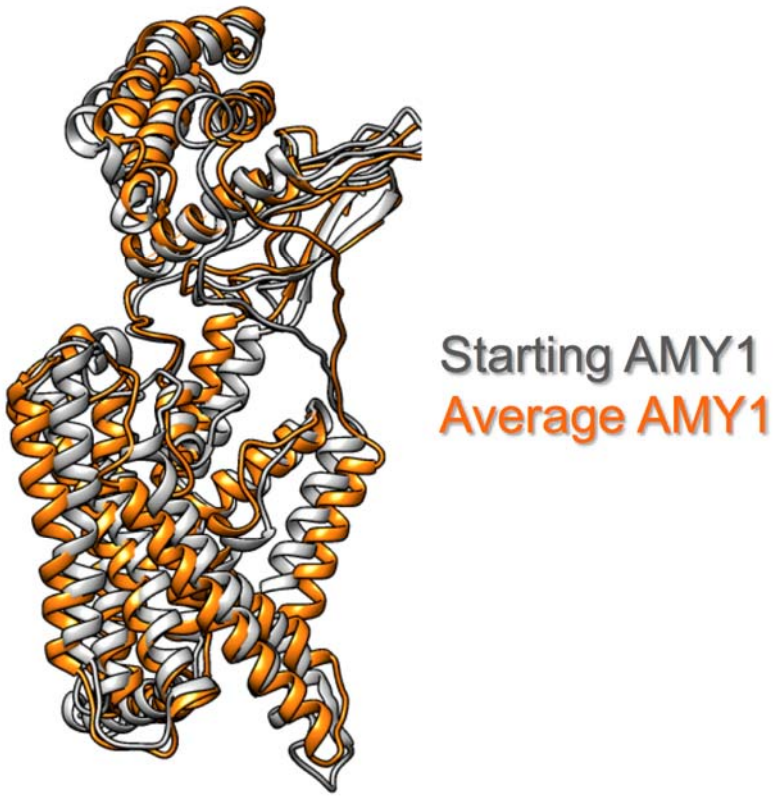

Supplementary modeling Fig. SM1
Superposition of the equilibrated AMY_1 receptor conformation (grey) and the average conformation (orange) from three MD replicas (total 750 ns).

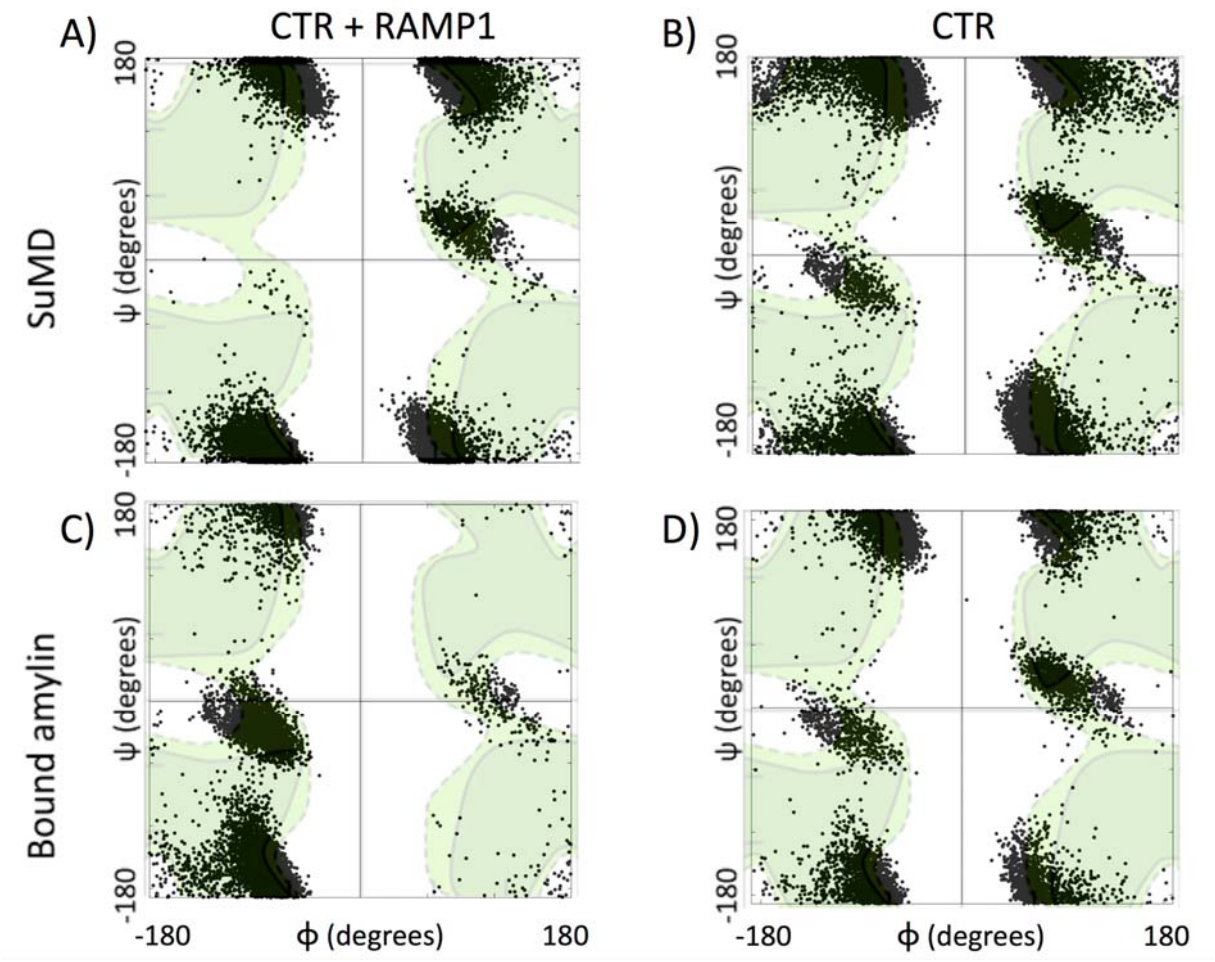

Supplementary modeling Fig. SM2
Ramachandran plots of amylin residue G33, during different MD simulations. (A) Amylin SuMD approach to the ECD of AMY_1 receptor; (B) amylin SuMD approach to the ECD of CTR receptor; (C) and (D) states sampled during simulations of the bound amylin in presence (C) and absence (D) of RAMP1. The minor tick marks denote angles in radians.

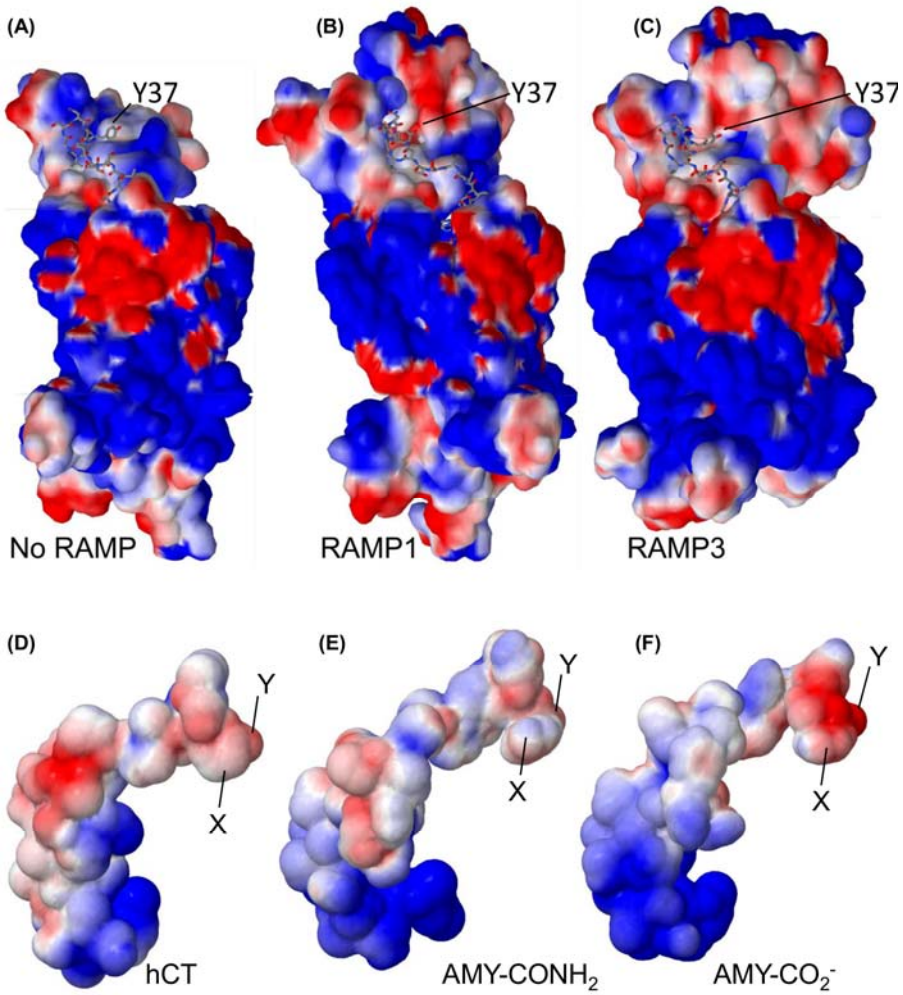

Supplementary modeling Fig. SM3
The molecular electrostatic potential (MEP) of the CTR. The MEP is colored between -2 kcal mol^{-1} (red) and +2 kcal mol^{-1} (blue). (A). The MEP of CTR in the absence of a RAMP. Human amylin-$CONH_2$ (C-terminus as amide) is shown in the structure but was not used to generate the MEP. (B). The MEP of CTR in the presence of RAMP1; as above, human amylin-$CONH_2$ is shown. (C). The MEP of CTR in the presence of RAMP3; as above, human amylin-$CONH_2$ is shown. (D). The MEP of human calcitonin. (E). The MEP of human amylin-$CONH_2$. (F). The MEP of human amylin-CO_2^-. For (A)–(C), the position of the C-terminal residue of amylin, Y37, is marked. For (A) this MEP is slightly positive (blue) at this position, which complements the somewhat negative potential at the C-terminus of human calcitonin shown in (D) (positions X (side chain) and Y (amide)). (B) Illustrates that in the presence of RAMP1, the MEP changes in several regions but becomes more negative in the region where Y37 binds; this complements the positive MEP on Y37 of amylin at position X shown in (E). The MEP remains negative around the amide of the peptide so that it is able to exploit the positive MEP around Ser129 on the ECD (Ser129 is the main amide anchor point amide); this region of positive MEP is reduced in the presence of RAMP1. (C) Illustrates that RAMP3 differentially effects the MEP on the receptor surface; the region around the Y37 binding site is less negative than in the presence of RAMP1. (F) Illustrates that the MEP around the C-terminus of the amylin-CO_2^- peptide is much more negative than for its amide counterpart.

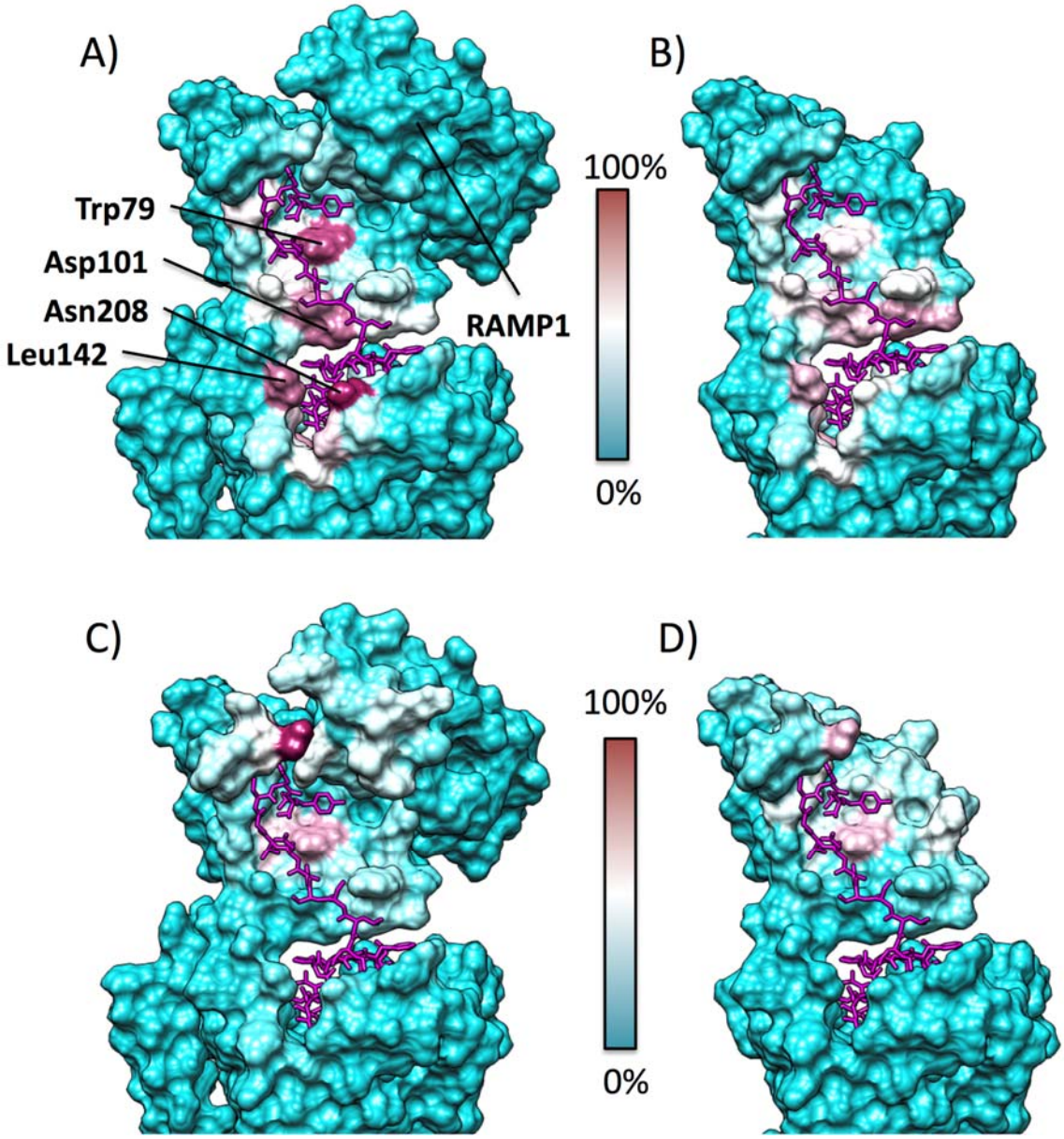

Supplementary modeling Fig. SM4
CTR/AMY$_1$ – amylin-amide (magenta) contacts identified during MD simulations, plotted on the CTR/AMY$_1$ molecular surface. The CTR/AMY$_1$ residues least engaged by amylin (0% contact) are colored cyan, while residues most engaged by amylin (100% contact) are colored purple. (A) MD simulations of amylin bound to the AMY$_1$ receptor. (B) MD simulations of amylin bound to CTR. (C) MD simulations of amylin after SuMD performed on the AMY$_1$ receptor. (D) MD simulations of amylin after SuMD performed on the CTR .

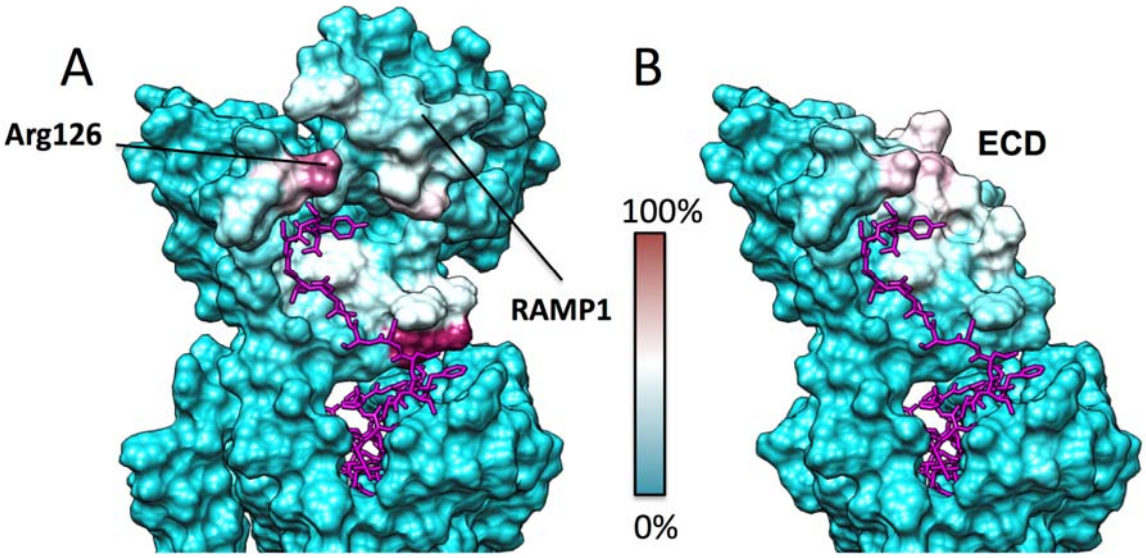

Supplementary modeling Fig. SM5
CTR/AMY$_1$ - amylin (magenta) contacts identified after SuMD simulations of carboxy-amylin plotted on the CTR/AMY$_1$ molecular surface. The CTR/AMY$_1$ residues least engaged by carboxy-amylin (0% contact) are colored cyan, while residues most engaged by amylin (100% contact) are colored purple. (A) MD simulations of carboxy-amylin after SuMD was performed on the AMY$_1$ receptor. (B) MD simulations of carboxy-amylin after SuMD was performed on the CTR.

Modeling Methodology

Model generation

The CTR-RAMP1-amylin complex model was generated using the cryo-electron microscopy structure of the CTR[1], the X-ray structure of the CTR ECD[2] and the X-ray structure of the CLR-RAMP1 ECD complex[3], combined using Modeller[4], as described elsewhere[5, 6]. The placement of the RAMP, described more fully elsewhere[5, 7], was determined by docking the RAMP1, RAMP2 and RAMP3 TM helix against active and inactive models of the calcitonin receptor-like receptor (CLR) using the Cluspro[8], Patchdock[9] and SwarmDock[10] servers. Results incompatible with the membrane topology were eliminated and the remaining structures were clustered and representatives from each cluster were scored using Firedock[11] so that the Cluspro, Patrhcdock and SwarmDock poses were treated equally. The best poses were redocked using Rosetta-Dock[12] and the consensus showed a preference to dock to TM7 of CLR, in agreement with experiment[13]. The RAMP TM docking was repeated for RAMP1, RAMP2 and RAMP3 against the active cryo-electron microscopy structure of CTR[14] using the Cluspro2, SwarmDock and Haddock[15] docking servers giving similar results. The basic model selected had the best DOPE score[16] out of 1000 models. The missing loop between the RAMP ECD and the RAMP transmembrane helix, ECL3 and the loop in amylin (c.f. CGRP[6]) were modelled using Modeller (2000 models, to generate the full structure) and the DOPE score for each loop model was determined and scaled between 0 and 1, with 1 corresponding to the best score. The accessibility for each structure, determined using half-sphere exposure[17], was scaled between 0 and 1, with 0 being the most conserved. The Pearson correlation between accessibility and the conservation, (from an in-house CTR multiple sequence alignment) was determined and the resultant correlation coefficients were scaled between 0 and 1. The product of the scaled DOPE score and the scaled correlation coefficients were used to identify modelled loops that satisfied the constraint of a low predicted empirical energy for which the conserved residues generally faced inwards[18] In order to improve the molecular dynamics (MD) simulation performance, the number of heavy atoms composing the AMY_1 receptor homology model were reduced, as elsewhere[5, 19], by retaining only the G protein atoms belonging to helix $\alpha 5$, the principle region responsible for activation. The RAMP *C*-terminus can affect signalling bias and so Ser141-Val148 were omitted from the RAMP1 to minimize any potential influence from this effect. The CTR coordinates were obtained by deleting RAMP1 from the AMY_1 homology model. The amylin *C*-terminus was generated in both the amidic form and the carboxylate form for both the AMY_1 and CTR receptors, giving a total of four different peptide - receptor complexes (Table SM1). The AMY_3 model was generated from the AMY_1 model using Modeller. Electrostatic potential calculations were carried out using APBSmem[20], as described elsewhere[6].

Molecular dynamics (MD) simulations

The systems were prepared for MD simulations by means of a multistep procedure that integrates both python htmd[21] and tcl (Tool Command Language) scripts. More precisely, the pdb2pqr[22] and propka[23] software were used to check the protein's structural integrity and to add hydrogen atoms (configurations of titratable amino acid side chains were visually inspected) appropriate for a simulated pH of 7.0. AMY_1 and CTR were embedded in rectangular matrixes of a 1-palmitoyl-2-oleyl-sn-glycerol-3-phospho-choline (POPC) bilayer (previously built by using the VMD Membrane Builder plugin 1.1, Membrane Plugin, Version 1.1. at http://www.ks.uiuc.edu/Research/vmd/plugins/membrane/) through an insertion method[24]: receptors were first oriented according to the CTR coordinates from the OPM database[25], then lipids overlapping the protein were removed and TIP3P water molecules[26] were added to the simulation box by means of the VMD Solvate plugin 1.5 (Solvate Plugin, Version 1.5. at <http://www.ks.uiuc.edu/Research/vmd/plugins/solvate/). Charge neutrality was finally reached by adding Na^+/Cl^- counter ions to a final concentration of 0.154 M, according to the VMD Autoionize plugin 1.3 (Autoionize Plugin, Version 1.3. at

<http://www.ks.uiuc.edu/Research/vmd/plugins/autoionize/). The CHARMM36 force field[27] was used.

Systems equilibration and classic MD run settings

All the following MD simulation stages were performed by using Acemd[28]. Equilibration of the four systems was achieved in isothermal-isobaric conditions (NPT) using the Berendsen barostat[29] (target pressure 1 atm) and the Langevin thermostat[30] (target temperature 300 K) with a low damping of 1 ps^{-1}. A three-stage procedure with an integration time step of 2 fs was performed: in the first one, 2000 conjugate-gradient minimization steps were applied to reduce the clashes between protein and lipids. Then, a 10 ns long MD simulation was performed in the NPT ensemble, with a positional constraint of 1 kcal mol^{-1} $Å^{-2}$ on protein and lipid phosphorus atoms. During the second stage, 30 ns of MD simulation in the NPT ensemble were performed constraining all protein atoms, but leaving the POPC residues free to diffuse in the bilayer. In the last equilibration stage, positional constraints were reduced by one half and applied only to the protein backbone alpha carbons, for a further 10 ns of MD simulation.

For each amylin - receptor complex, three 250 ns long unbiased MD replicas were run, for a total of twelve trajectories (Table SM1). Production MD trajectories were computed with an integration time step of 4 fs in the canonical ensemble (NVT) at 300 K, using a thermostat damping of 0.1 ps^{-1} and the M-SHAKE algorithm[31] to constrain the bond lengths involving hydrogen atoms. The cut off distance for electrostatic interactions was set at 9 Å, with a switching function applied beyond 7.5 Å. Long range Coulomb interactions were handled using the particle mesh Ewald summation method (PME) [32] by setting the mesh spacing to 1.0 Å.

Metadynamics simulations.

Despite the relatively high sequence identity between amylin and calcitonin (the template for amylin modeling in its bound state), the possibility that structural side chain differences may lead to slightly different binding modes should not be excluded. Unfortunately, during classic unbiased MD simulations alternative stable bound and metastable states cannot be easily sampled, due to the kinetic barriers that may separate two energy minima. Metadynamics simulations[33, 34] were therefore performed to (i) investigate alternative bound amylin states and (ii) to model contacts with the receptor along the dissociation path. Metadynamics can be summarized as the seeding, at discrete time intervals, of a history–dependent energetic term centred along a predefined set of collective variables (CVs) able to describe the evolution of the system. When the energetic bias is added at a certain instant, the probability that the system will revisit that specific configuration is decreased according to the shape of the supplied energetic Gaussian function. Thanks to this theoretical approach it is possible to fill energy minimum on the energy surface defined by the CVs, therefore increasing the transition probability between different energy minima[34]. Before performing a metadynamics simulation it is therefore necessary to define one or more CVs able to describe the system transition of interest. Here the distance between the geometrical centres of the amylin *N*-terminal helical portion (residues 1 to 17) and the CTR transmembrane bundle domain (residues 140 to 395) was biased. The use of a similar ligand - receptor distance as CV during unbinding simulations has been successfully applied[35] to class A GPCRs. Here, the Gaussian height and width were set at 0.01 kcal/mol and 0.1 Å respectively, with depositions done every 1 ps, using Plumed 2.3[36], as a plugin to Acemd[28]. Simulations proceeded until the peptide *N*-terminus distance from the starting bound state was at least 15 Å. The partial unbinding metadynamics replicas were collected on each amylin complex for a total of twelve trajectories (Table SM1).

Supervised MD (SuMD)

To generate the starting coordinates for SuMD, the last frame from one partial unbinding metadynamics simulation was extracted and the peptide was translated in the Cartesian space

according to the arbitrary vector (0 Å; -30 Å; 30 Å), by using VMD. Resulting systems were then prepared for simulations and equilibrated as reported in the previous section.

The SuMD approach has been successfully applied to the binding of small molecules to their biological target[37-40] and, more recently, it has been also proposed for modeling recognition events of peptides[41]. According to this MD-based approach, the timescale needed to reproduce complete intermolecular complex formation results in the time scale of nanoseconds, instead of hundreds of nanoseconds or microseconds usually necessary with unsupervised MD. Sampling is gained without the introduction of any bias by applying a tabu–like algorithm to monitor the distance between the centres of masses (or the geometrical centres) of the ligand and the binding site during short classical MD simulations. More precisely, SuMD considers the ligand atoms and the atoms of user-defined protein residues to monitor the distance between the center of masses of the binder and the binding site. A series of unbiased MD simulations are performed and after each simulation the distance points (collected at regular time intervals) are fitted into a linear function. If the resulting slope is negative the next simulation step starts from the last set of coordinates and velocities produced, otherwise the simulation is restarted by randomly assigning the atomic velocities. From a general point of view, SuMD can be considered an adaptive sampling method[42] during which unbiased simulation are run consecutively. In the present work, the target binding site was defined by the geometrical centres of CTR residues Asp77, Gly78, Trp79, Trp128, Ser129 and Tyr131, while amylin C-terminus residues T36 and Y37 were considered for the ligand. The duration of the time windows considered for supervision was set to 1 ns, while distance points were collected every 10 ps using Plumed 2.3. For each replica, when the distance between the two centres of mass reached a value lower than 8 Å, a classic unsupervised MD simulation was performed for a further 30 ns to allow the system to sample local energetic minima.

For each peptide - receptor system, at least ten replicas were performed, as summarized in (Table SM1).

SuMD Analysis

SuMD trajectories were joined using the Prody[43] python package. Amylin contacts and hydrogen bonds were quantified using VMD[44]. A contact between two residues was considered productive if at least two atoms were detected at distances less than 3.5 Å. A distance between acceptor and donor atoms of 3 Å and an angle value of 20° were set as the geometrical cut-off for hydrogen bonds.

The MMPBSA.py[45] script, from the AmberTools17 suite (The Amber Molecular Dynamics Package. at http://ambermd.org/), was used to compute molecular mechanics energies combined with the generalized Born and surface area continuum solvation (MM/GBSA) method, after transforming the CHARMM psf topology files to an Amber prmtop format using Parmed (ParmEd — ParmEd documentation. at <http://parmed.github.io/ParmEd/html/index.html).

Sequence alignments, equilibrated coordinates, topology files and tables reassuming the contacts computed during all the simulations are available from http://researchdata.essex.ac.uk/76/, doi:0.5526/ERDR-00000076.

Analyzing differences in the bound amylin trajectories

Differences in the distribution of the ψ,ϕ torsional angles that define the protein backbone conformation were evaluated for each residue using the Hellinger distance (HD):

$$HD = \frac{1}{\sqrt{2}}(\sqrt{P} - \sqrt{Q})^2$$

where P, the distribution of ϕ values in the simulations with no RAMP and Q, the distribution of ϕ values in the simulations with RAMP, were evaluated from the molecular dynamics trajectories of

the CTR-amylin-C-terminal helix of Gs complex in the presence and absence of RAMP1. A similar metric was evaluated for the ψ values. Figure 5 shows the higher computed value between ϕ or ψ, in order to highlight the most significant conformational differences, Metrics for van der Walls contacts and hydrogen bonds were evaluated considering the difference between the total numbers of contacts during the simulations in presence and absence of RAMP1.

Table SM1. Summary of all the MD simulations performed in the present work.

SYSTEM	AMY_1 (CTR + RAMP1)		CTR (no RAMP)	
Amylin C terminus	Amide	Carboxylate	Amide	Carboxylate
Unbiased MD bound state	3 replicas (750 ns)	3 replicas (750 ns)	3 replicas (750 ns)	3 replicas (750 ns)
Partial unbinding metadynamics	3 replicas (79 ns)	3 replicas (58 ns)	3 replicas (55 ns)	3 replicas (59 ns)
Supervised MD	10 replicas (242 ns / 705 ns tot)	10 replicas (235 ns / 670 ns tot)	12 replicas (239 ns / 630 ns tot)	10 replicas (473 ns / 704 ns tot)
Unsupervised MD (metastable states sampling)	300 ns (10 x 30 ns)	300 ns (10 x 30 ns)	360 ns (12 x 30 ns)	300 ns (10 x 30 ns)

References

[1] Liang, Y. L., Khoshouei, M., Radjainia, M., Zhang, Y., Glukhova, A., Tarrasch, J., Thal, D. M., Furness, S. G. B., Christopoulos, G., Coudrat, T., Danev, R., Baumeister, W., Miller, L. J., Christopoulos, A., Kobilka, B. K., Wootten, D., Skiniotis, G., and Sexton, P. M. (2017) Phase-plate cryo-EM structure of a class B GPCR-G-protein complex, *Nature 546*, 118-+. 10.1038/nature22327

[2] Johansson, E., Hansen, J. L., Hansen, A. M. K., Shaw, A. C., Becker, P., Schaffer, L., and Reedtz-Runge, S. (2016) Type II Turn of Receptor-bound Salmon Calcitonin Revealed by X-ray Crystallography, *Journal of Biological Chemistry 291*, 13689-13698. 10.1074/jbc.M116.726034

[3] Booe, J. M., Walker, C. S., Barwell, J., Kuteyi, G., Simms, J., Jamaluddin, M. A., Warner, M. L., Bill, R. M., Harris, P. W., Brimble, M. A., Poyner, D. R., Hay, D. L., and Pioszak, A. A. (2015) Structural Basis for Receptor Activity-Modifying Protein-Dependent Selective Peptide Recognition by a G Protein-Coupled Receptor, *Molecular Cell 58*, 1040-1052. 10.1016/j.molcel.2015.04.018

[4] Eswar, N., Webb, B., Marti-Renom, M. S., Madhusudham, D. E., Shen, M. Y., Pieper, U., and Sali, A. (2007) Comparative Protein Structure Modeling with MODELLER, *Current Protocols in Bioinformatics*, 2.9.1-2.9.31.

[5] Weston, C., Winfield, I., Harris, M., Hodgson, R., Shah, A., Dowell, S. J., Mobarec, J. C., Woodlock, D. A., Reynolds, C. A., Poyner, D. R., Watkins, H. A., and Ladds, G. (2016) Receptor Activity-modifying Protein-directed G Protein Signaling Specificity for the Calcitonin Gene-related Peptide Family of Receptors, *J Biol Chem 291*, 21925-21944. 10.1074/jbc.M116.751362

[6] Watkins, H. A., Chakravarthy, M., Abhayawardana, R. S., Gingell, J. J., Garelja, M., Pardamwar, M., McElhinney, J. M., Lathbridge, A., Constantine, A., Harris, P. W., Yuen, T. Y., Brimble, M. A., Barwell, J., Poyner, D. R., Woolley, M. J., Conner, A. C., Pioszak, A. A., Reynolds, C. A., and Hay, D. L. (2016) Receptor Activity-modifying Proteins 2 and 3 Generate Adrenomedullin Receptor Subtypes with Distinct Molecular Properties, *J Biol Chem 291*, 11657-11675. 10.1074/jbc.M115.688218

[7] Watkins, H. A., Chakravarthy, M., Abhayawardana, R. S., Gingell, J. J., Garelja, M., Pardamwar, M., McElhinney, J. M. W. R., Lathbridge, A., Constantine, A., Harris, P. W. R., Yuen, T.-Y., Brimble, M. A., Barwell, J., Poyner, D. R., Woolley, M. J., Conner, A. C., Pioszak, A. A., Reynolds, C. A., and Hay, D. L. (2016) Receptor Activity-modifying Proteins 2 and 3 Generate Adrenomedullin Receptor Subtypes with Distinct Molecular Properties, *The Journal of Biological Chemistry 291*, 11657-11675. 10.1074/jbc.M115.688218

[8] Mirzaei, H., Zarbafian, S., Villar, E., Mottarella, S., Beglov, D., Vajda, S., Paschalidis, I., Vakili, P., and Kozakov, D. (2015) Energy Minimization on Manifolds for Docking Flexible Molecules, *J Chem Theory Comput 11*, 1063-1076. 10.1021/ct500155t

[9] Schneidman-Duhovny, D., Inbar, Y., Nussinov, R., and Wolfson, H. J. (2005) PatchDock and SymmDock: servers for rigid and symmetric docking, *Nucleic Acids Res 33*, W363-367. 10.1093/nar/gki481

[10] Torchala, M., Moal, I. H., Chaleil, R. A., Fernandez-Recio, J., and Bates, P. A. (2013) SwarmDock: a server for flexible protein-protein docking, *Bioinformatics 29*, 807-809. 10.1093/bioinformatics/btt038

[11] Mashiach, E., Schneidman-Duhovny, D., Andrusier, N., Nussinov, R., and Wolfson, H. J. (2008) FireDock: a web server for fast interaction refinement in molecular docking, *Nucleic Acids Res 36*, W229-232. 10.1093/nar/gkn186

[12] Chaudhury, S., Berrondo, M., Weitzner, B. D., Muthu, P., Bergman, H., and Gray, J. J. (2011) Benchmarking and analysis of protein docking performance in Rosetta v3.2, *PLoS One 6*, e22477. 10.1371/journal.pone.0022477

[13] Harikumar, K. G., Simms, J., Christopoulos, G., Sexton, P. M., and Miller, L. J. (2009) Molecular Basis of Association of Receptor Activity-Modifying Protein 3 with the Family B G Protein-Coupled Secretin Receptor, *Biochemistry 48*, 11773-11785. 10.1021/bi901326k
[14] Liang, Y. L., Khoshouei, M., Radjainia, M., Zhang, Y., Glukhova, A., Tarrasch, J., Thal, D. M., Furness, S. G. B., Christopoulos, G., Coudrat, T., Danev, R., Baumeister, W., Miller, L. J., Christopoulos, A., Kobilka, B. K., Wootten, D., Skiniotis, G., and Sexton, P. M. (2017) Phase-plate cryo-EM structure of a class B GPCR-G-protein complex, *Nature 546*, 118-123. 10.1038/nature22327
[15] van Zundert, G. C. P., Rodrigues, J., Trellet, M., Schmitz, C., Kastritis, P. L., Karaca, E., Melquiond, A. S. J., van Dijk, M., de Vries, S. J., and Bonvin, A. (2016) The HADDOCK2.2 Web Server: User-Friendly Integrative Modeling of Biomolecular Complexes, *J Mol Biol 428*, 720-725. 10.1016/j.jmb.2015.09.014
[16] Shen, M. Y., and Sali, A. (2006) Statistical potential for assessment and prediction of protein structures, *Protein Sci. 15*, 2507-2524.
[17] Hamelryck, T. (2005) An amino acid has two sides: A new 2D measure provides a different view of solvent exposure, *Proteins-Structure Function and Bioinformatics 59*, 38-48. 10.1002/prot.20379
[18] Baldwin, J. M., Schertler, G. F., and Unger, V. M. (1997) An alpha-carbon template for the transmembrane helices in the rhodopsin family of G-protein-coupled receptors, *Journal of Molecular Biology 272*, 144-164.
[19] Wootten, D., Reynolds, C. A., Smith, K. J., Mobarec, J. C., Koole, C., Savage, E. E., Pabreja, K., Simms, J., Sridhar, R., Furness, S. G., Liu, M., Thompson, P. E., Miller, L. J., Christopoulos, A., and Sexton, P. M. (2016) The Extracellular Surface of the GLP-1 Receptor Is a Molecular Trigger for Biased Agonism, *Cell 165*, 1632-1643. 10.1016/j.cell.2016.05.023
[20] Callenberg, K. M., Choudhary, O. P., de Forest, G. L., Gohara, D. W., Baker, N. A., and Grabe, M. (2010) APBSmem: a graphical interface for electrostatic calculations at the membrane, *PLoS One. 5*.
[21] Doerr, S., Harvey, M. J., Noe, F., and De Fabritiis, G. (2016) HTMD: High-Throughput Molecular Dynamics for Molecular Discovery, *Journal of Chemical Theory & Computation 12*, 1845-1852. 10.1021/acs.jctc.6b00049
[22] Dolinsky, T. J., Nielsen, J. E., McCammon, J. A., and Baker, N. A. (2004) PDB2PQR: an automated pipeline for the setup of Poisson-Boltzmann electrostatics calculations, *Nucleic Acids Res 32*, W665-W667.
[23] Li, H., Robertson, A. D., and Jensen, J. H. (2005) Very fast empirical prediction and rationalization of protein pKa values, *Proteins 61*, 704-721. 10.1002/prot.20660
[24] Sommer, B. (2013) Membrane Packing Problems: A short Review on computational Membrane Modeling Methods and Tools, *Comput Struct Biotechnol J 5*, e201302014. 10.5936/csbj.201302014
[25] Lomize, M. A., Lomize, A. L., Pogozheva, I. D., and Mosberg, H. I. (2006) OPM: orientations of proteins in membranes database, *Bioinformatics 22*, 623-625. 10.1093/bioinformatics/btk023
[26] Jorgensen, W. L., Chandrasekhar, J., Madura, J. D., Impey, R. W., and Klein, M. L. (1983) Comparison of Simple Potential Functions for Simulating Liquid Water, *J.Chem.Phys. 79*, 926-935.
[27] Huang, J., and MacKerell, A. D., Jr. (2013) CHARMM36 all-atom additive protein force field: validation based on comparison to NMR data, *J Comput Chem 34*, 2135-2145. 10.1002/jcc.23354

[28] Harvey, M. J., Giupponi, G., and De Fabritiis, G. (2009) ACEMD: Accelerating Biomolecular Dynamics in the Microsecond Time Scale, *Journal of Chemical Theory & Computation 5*, 1632-1639. 10.1021/ct9000685
[29] Berendsen, H. J. C., Postma, J. P. M., Vangunsteren, W. F., Dinola, A., and Haak, J. R. (1984) Molecular-Dynamics with Coupling to an External Bath, *Journal of Chemical Physics 81*, 3684-3690. Doi 10.1063/1.448118
[30] Loncharich, R. J., Brooks, B. R., and Pastor, R. W. (1992) Langevin dynamics of peptides: the frictional dependence of isomerization rates of N-acetylalanyl-N'-methylamide, *Biopolymers 32*, 523-535. 10.1002/bip.360320508
[31] Krautler, V., Van Gunsteren, W. F., and Hunenberger, P. H. (2001) A fast SHAKE: Algorithm to solve distance constraint equations for small molecules in molecular dynamics simulations, *Journal of Computational Chemistry 22*, 501-508. Doi 10.1002/1096-987x(20010415)22:5<501::Aid-Jcc1021>3.0.Co;2-V
[32] Essmann, U., Perera, L., Berkowitz, M. L., Darden, T., Lee, H., and Pedersen, L. G. (1995) A Smooth Particle Mesh Ewald Method, *Journal of Chemical Physics 103*, 8577-8593. Doi 10.1063/1.470117
[33] Valsson, O., Tiwary, P., and Parrinello, M. (2016) Enhancing Important Fluctuations: Rare Events and Metadynamics from a Conceptual Viewpoint, *Annu Rev Phys Chem 67*, 159-184. 10.1146/annurev-physchem-040215-112229
[34] Barducci, A., Bonomi, M., and Parrinello, M. (2011) Metadynamics, *Wiley Interdisciplinary Reviews-Computational Molecular Science 1*, 826-843. 10.1002/wcms.31
[35] Saleh, N., Ibrahim, P., Saladino, G., Gervasio, F. L., and Clark, T. (2017) An Efficient Metadynamics-Based Protocol To Model the Binding Affinity and the Transition State Ensemble of G-Protein-Coupled Receptor Ligands, *Journal of Chemical Information & Modeling 57*, 1210-1217. 10.1021/acs.jcim.6b00772
[36] Tribello, G. A., Bonomi, M., Branduardi, D., Camilloni, C., and Bussi, G. (2014) PLUMED 2: New feathers for an old bird, *Computer Physics Communications 185*, 604-613. 10.1016/j.cpc.2013.09.018
[37] Deganutti, G., Cuzzolin, A., Ciancetta, A., and Moro, S. (2015) Understanding allosteric interactions in G protein-coupled receptors using Supervised Molecular Dynamics: A prototype study analysing the human A3 adenosine receptor positive allosteric modulator LUF6000, *Bioorg Med Chem 23*, 4065-4071. 10.1016/j.bmc.2015.03.039
[38] Sabbadin, D., and Moro, S. (2014) Supervised molecular dynamics (SuMD) as a helpful tool to depict GPCR-ligand recognition pathway in a nanosecond time scale, *J Chem Inf Model 54*, 372-376. 10.1021/ci400766b
[39] Cuzzolin, A., Sturlese, M., Deganutti, G., Salmaso, V., Sabbadin, D., Ciancetta, A., and Moro, S. (2016) Deciphering the Complexity of Ligand-Protein Recognition Pathways Using Supervised Molecular Dynamics (SuMD) Simulations, *J Chem Inf Model 56*, 687-705. 10.1021/acs.jcim.5b00702
[40] Deganutti, G., Welihinda, A., and Moro, S. (2017) Comparison of the Human A2A Adenosine Receptor Recognition by Adenosine and Inosine: New Insight from Supervised Molecular Dynamics Simulations, *ChemMedChem 12*, 1319-1326. 10.1002/cmdc.201700200
[41] Salmaso, V., Sturlese, M., Cuzzolin, A., and Moro, S. (2017) Exploring Protein-Peptide Recognition Pathways Using a Supervised Molecular Dynamics Approach, *Structure 25*, 655-662 e652. 10.1016/j.str.2017.02.009
[42] Deganutti, G., and Moro, S. (2017) Estimation of kinetic and thermodynamic ligand-binding parameters using computational strategies, *Future Med Chem 9*, 507-523. 10.4155/fmc-2016-0224
[43] Bakan, A., Meireles, L. M., and Bahar, I. (2011) ProDy: protein dynamics inferred from theory and experiments, *Bioinformatics 27*, 1575-1577. 10.1093/bioinformatics/btr168

[44] Humphrey, W., Dalke, A., and Schulten, K. (1996) VMD: visual molecular dynamics, *J Mol.Graph. 14*, 33-38.
[45] Miller, B. R., McGee, T. D., Swails, J. M., Homeyer, N., Gohlke, H., and Roitberg, A. E. (2012) MMPBSA.py: An Efficient Program for End-State Free Energy Calculations, *Journal of Chemical Theory & Computation 8*, 3314-3321. 10.1021/ct300418h